LA-UR-04- 1791

*Approved for public release;*
*distribution is unlimited.*

*Title:* MULTIPHASE FLOW SIMULATION OF IGNITION OF SOLID EXPLOSIVE

*Author(s):* Qisu Zou, Duan Z. Zhang, Nely T. Padial-Collins, and W. Brian VanderHeyden, Fluid Dynamics Group (T-3), Theoretical Division

*Submitted to:* 5th International Conference on Multiphase Flow, ICMF '04
Yokohama, JAPAN
30MAY - 4 JUN 2004



Los Alamos
NATIONAL LABORATORY

5th International Conference on Multiphase Flow, ICMF'04
Yokohama, Japan, May 30–June 4, 2004
Paper No. 239

# Multiphase Flow Simulation of Ignition of Solid Explosive

**Qisu Zou, Duan Z. Zhang, Nely T. Padial-Collins and W. Brian VanderHeyden**

Los Alamos National Laboratory, T-3, B216, Los Alamos, NM, 87545, USA, qisu@lanl.gov

**Abstract** Ignition of a solid explosive involves chemical reaction, phase change, heat, mass and momentum transfers between the solid explosive and the product gas. To simulate the motion of the solid material Lagrangian method is needed to trace the deformation of the material. Calculation of the large deformation involved in the gas and the solid materials demands an Eulerian method to avoid mesh tangling issues that cripple conventional Lagrangian methods. To satisfy the demands for both Lagrangian and Eulerian methods, a particle-in-cell (PIC) method is adopted. While the method is computationally expensive compared to other numerical methods, it offers unique capability of combining the advantages of the Lagrangian and Eulerian treatments in handling material deformations. When the method is applied to multiphase flows, it can solve many complicated multi-material flow problems that are extremely difficult or impossible for other methods. Ignition of a solid explosive is such a problem. In the present paper we use a two-phase flow model based on available experimental data and commonly used momentum and thermal coupling models to investigate the ignition mechanisms and processes in a solid explosive material. Despite unresolved uncertainties in the model, results obtained are in qualitative agreements with experimental data.

## 1. Introduction

It is generally agreed that explosion of an explosive material is initiated by small high temperature regions, called hot spots, with a size of about a few microns to a few hundred microns. Despite progresses in the study of generation of hot spots (Bennett et al. 1998, Hackett et al., 2000, Kang and Butler, 1992, Mellor et al., 1995, Browning et al., 2003), the mechanisms leading to generation of hot spots are not well understood. Unintended explosions happen. Generation of hot spots does not necessary lead to an explosion. In some experiments significant burn marks and puffs of smoke are observed without explosion. In one experiment an explosive material fizzled for several minutes before violent explosion occurred.

Initiation of an explosion in a solid involves complicated mechanical and chemical processes. The processes involve heat, mass and momentum transfers at various length and time scales. The local pressure spike generated around the hot spot as a result of rapid gas production from chemical reactions drives the motion of the solid explosive. A solid explosive is typically a porous material with a few percent volume fraction of air. Around a hot spot both temperature and pressure are high. Induced gas motion has two competing effects. Gas motion can carry away heat and reduce the local temperature and reduce the tendency for explosion. On the other hand, gas motion can also spread heat around and enhance interactions among hot spots and then increase the chance of an explosion. The pressure around the hot spot can cause motion of the solid explosive and cause fracture and growth of the gas pores. Therefore ignition of explosion in a solid material is a complicated fluid-structure interaction problem. It poses a significant challenge to computation fluid dynamics and to modeling the complicated physics and chemistry involved.

To ensure the safety of explosive materials we are investigating possible explosion mechanisms. One of the possible mechanisms we are investigating is the effect of sand grit on

a surface against which an explosive material slides. It is estimated that the temperature of the explosive material around the grit can be hot enough and last a sufficient duration to cause significant chemical reactions. The present work investigates conditions under which hot spots can lead to an explosion. An averaged field approached is adopted. To simplify numerical simulation we do not distinguish the air initially in the material and the gas produced due to chemical reaction. Solid and gas are treated as interpenetrating continuums. The motion of the solid is driven by the divergence of the stress in the solid and by the interaction forces between the solid and gas. The stress in the solid is calculated by using Hooke's law with a von Mises yield condition. The stress in the solid is a function of the strain. The calculation of the stress requires following the history of the solid deformation, this presents significant difficulties to a numerical scheme based solely on an Eulerian grid. If a Lagrangian grid is used to trace the motion of the solid, besides possible mesh tangling issues faced by Lagrangian methods for large deformation motions, another grid system must be set up for the gas motion, because the gas and the solid have two different velocity fields. To avoid these difficulties, we use a particle in cell (PIC) method. In the method the gas phase is computed on an Eulerian grid and the solid phase is computed on particles on the same Eulerian grid. The particles are Lagrangian points of the solid material. History information of the solid phase is carried on the particles. Information about the solid phase is interpolated back and forth between particle and the Eulerian grid. Although this method is expensive for many simple problems, the flexibility of the method offers unique capabilities in solving difficult problems, such as the one studied in this paper, where other methods encounter difficulties.

The work of Guilkey et al. (2004) takes a similar approach to a related problem. The major difference in this work and in theirs is: (1) in this work, a single set of integrated code (Cartablanca, VanderHeyden et al., 2000) is used. (2) some models, like a subgrid chemical reaction model and careful treatment of momentum and energy coupling, are introduced in this work. Without the careful treatment of the coupling terms, some of the phenomena cannot be simulated.

Section 2 presents the averaged equations, section 3 is a discussion of some subgrid models and coupling models. Section 4 discusses the particle method, the simulation results are presented in section 5, A summary is given in Section 6. The values of the physical quantities used are listed in the Appendix.

## 2. Averaged Equations

As mention in the Introduction, the solid explosive material is a porous material. In an explosion, not only gas but also the solid moves. Therefore we need to treat the problem as a general two-phase flow. The mass conservation equation is written as

$$\begin{aligned} &\frac{\partial \theta_s \rho_s}{\partial t} + \nabla \cdot \theta_s \rho_s \mathbf{u}_s = -\dot{m}_g \\ &\frac{\partial \theta_g \rho_g}{\partial t} + \nabla \cdot \theta_g \rho_g \mathbf{u}_g = \dot{m}_g \\ &\dot{m}_g = \theta_s \rho_s R \end{aligned} \tag{1}$$

where $\rho$ is the density, $\theta$ is the volume fraction, $\mathbf{u}$ is the velocity and $R$ is the rate of chemical reaction. Subscripts s and g used in these equations indicate the solid phase and the gas phase. Although, there are several chemical reaction steps involved before the solid explosive becomes the product gas, the intermediate products only exist in a very thin combustion front. The length scale of the combustion front is much smaller than the practical cell size used in a calculation. Thus, the reaction rate in a solid can be modeled based on the Arrhenius law:

$$R = Z\exp(-E/R^0 T_s) \tag{2}$$

with an effective frequency factor Z and an effect activation energy E to account for combined effects of multi-step chemical reactions (Henson et al., 2002). $R^0$ is the universal

gas constant. The values used in this work is listed in the Appendix. This kind of one-step chemical reaction model has been used to calculate combustion of solids as a reaction term in the Frank-Kamenetskii equation

$$\rho C_p \frac{\partial T}{\partial t} - K_s \Delta T = Z \exp(-E / \mathrm{R}^0 T) \tag{3}$$

where $C_p$ is the heat capacity of the solid, and $K_s$ is the thermal conductivity of the solid (Boddington, 1962). However such a chemical reaction rate cannot be used directly for our purpose, because the rapid chemical reaction of the explosive material results in a thin combustion wave front. The thickness of the wave front ranges from a few microns to a few hundred microns depending on the temperature. For an engineering problem, resolving this length scale is impractical and subgrid chemical reaction models need to be developed as discussed in Section 3, where a model for calculating $R$ in Eq. (1) is given.

The momentum equations for both phases are written as

$$\frac{\partial \rho_s \theta_s \mathbf{u}_s}{\partial t} + \nabla \cdot \rho_s \theta_s \mathbf{u}_s \mathbf{u}_s = -\theta_s \nabla p + \theta_s \theta_g K_{gs} (\mathbf{u}_g - \mathbf{u}_s) + \nabla \cdot \theta_s (\boldsymbol{\sigma}_s - p\mathbf{I}) - \dot{m}_g \mathbf{u}_s \tag{4}$$

$$\frac{\partial \rho_g \theta_g \mathbf{u}_g}{\partial t} + \nabla \cdot \rho_g \theta_g \mathbf{u}_g \mathbf{u}_g = -\theta_g \nabla p + \theta_s \theta_g K_{gs} (\mathbf{u}_s - \mathbf{u}_g) + \theta_g \nabla \cdot (\boldsymbol{\tau}_g) + \dot{m}_g \mathbf{u}_s, \tag{5}$$

where p is the pressure of the gas phase, $\boldsymbol{\sigma}_s$ is the solid stress, $\boldsymbol{\tau}_g$ is the deviatoric stress tensor based on the gas velocity $\mathbf{u}_g$. The stress in the solid is related to the strain and strain rate $\dot{\boldsymbol{\varepsilon}}$ as:

$$\boldsymbol{\sigma}_s = -[p_s + \mu_2 tr(\dot{\boldsymbol{\varepsilon}})]\mathbf{I} + 2\mu[\dot{\boldsymbol{\varepsilon}} - \frac{1}{n_d} tr(\dot{\boldsymbol{\varepsilon}})\mathbf{I}] + \boldsymbol{\tau}_s \tag{6}$$

where $\mu_2$ is the bulk viscosity, $\mu$ is the shear viscosity, and $n_d$ is the space dimension. The solid pressure $p_s$, is determined by the equation of state of the solid material. The second term is represents the viscosity of the solid and the last term is a traceless stress related to deformation as

$$\frac{\partial \boldsymbol{\tau}_s}{\partial t} + \mathbf{u}_s \cdot \nabla \boldsymbol{\tau}_s = 2G[\dot{\boldsymbol{\varepsilon}} - \frac{1}{n_d} tr(\dot{\boldsymbol{\varepsilon}})\mathbf{I}] \tag{7}$$

where G is the shear modulus of the solid. The stress $\boldsymbol{\tau}_s$ is calculated following the motion of the solid. A von Mises yield condition of the stress is enforced as given in Section 4.

We assume that the momentum coupling is through the drag only and $K_{gs}$ is the drag coefficient to be discussed in Section 3. We also assume that the newly produced gas carries the momentum of its original phase, that is the momentum of the solid phase in this case.

The energy equations are written in terms of enthalpy, $h$:

$$\frac{\partial \rho_s \theta_s h_s}{\partial t} + \nabla \cdot \rho_s \theta_s h_s \mathbf{u}_s = K_e \theta_s \theta_g (T_g - T_s) - h_s \dot{m}_g \tag{8}$$

$$\frac{\partial \rho_g \theta_g h_g}{\partial t} + \nabla \cdot \rho_g \theta_g h_g \mathbf{u}_g = \frac{Dp}{Dt} + \boldsymbol{\tau}_g : \nabla \mathbf{u}_g + K_e \theta_s \theta_g (T_g - T_s) + h_s \dot{m}_g \tag{9}$$

where $K_e$ is a coupling coefficient representing the heat exchange between two phases to be discussed in Section 3. $\dot{\varepsilon}_p$ is the rate of plastic deformation. The temperature is related to the enthalpy as

$$h_k = h_k^f + C_{pk}(T - T^f), \quad k = g \text{ or } s \tag{10}$$

where $h_k^f$ is the enthalpy formation, $T^f$ is the temperature formation. In principle the enthalpy for the solid should include the elastic energy stored in the material. Equation (8) only accounts for the thermal part of the enthalpy. In the examples shown in Section 5, the solid explosive is converted to gas before the yield stress is reached, therefore the last term in the equation (8) can be neglected. The density and heat capacity of the gas is much smaller than those of the solid phase, therefore the enthalpy change results from the pressure and viscous dissipation need to be accounted for in Eq. (9). As in the momentum equations we assume that the newly produced gas carries the enthalpy of its original solid phase. During an ignition the heat conduction is small compared to the heat convection and heat generation from the chemical reaction, thus we neglect the conduction terms in the energy equation above.

The equation of state for the solid is an equation based on Hooke's law with a thermal expansion effect:

$$\rho_s = \frac{eosA + eosB\, p_s}{1+\beta_e(T-T_0)}, \qquad (11)$$
$$\beta_e = 1.47\times10^{-4}\ 1/K, \quad T_0 = 300\,\mathrm{K}.$$

The value of the coefficient of volumetric expansion $\beta_e$ is from Menikoff and Sewall (2002).

The coefficient *eosB* is related to the bulk modulus *B* of the solid by:

$$eosB = \rho_0 / B,$$

where $\rho_0$ is the solid density at standard states. The equation of state for the gas is the ideal gas law:

$$\rho_g = B_g p / T, \qquad (12)$$

## 3. Subgrid models and coupling terms

In this, section, we develop a subgrid chemical reaction model and the momentum coupling and energy coupling models. To develop the subgrid chemical reaction model, we first study the combustion wave speed. To obtain the wave speed one can seek a traveling wave solution to the Frank-Kamenetskii equation (Barenblatt, 1996). The nonlinearity of the equation results in a nonlinear eigenvalue problem. Instead using a complicated mathematical process to find the traveling wave solution, we estimate it as follows. Let w be the thickness of combustion wave front and $u_c$ be the combustion wave speed. The time it takes the combustion wave to travel through the thickness w is $\Delta t = w/u_c$. During this time the thermal diffusion heats a region in front of the wave. The thickness of the heated region is $\sqrt{D_s w/u_c}$, where $D_s = K_s/\rho_s C_{ps}$ is the thermal diffusivity of the solid. To have a steady wave front, this region heated by thermal diffusion, should be the same as the thickness w. Therefore we have $w = \sqrt{D_s w/u_c}$ or $w = D_s/u_c$. The rate of the material consumption can be calculated as $w/\Delta t = u_c$. The rate of the material consumption can also be calculated using the rate of chemical reaction as $\int_0^w Z\exp(-E/\mathrm{R}^0T)dx$. Therefore we have

$$u_c = \int_0^w Z\exp(-E/\mathrm{R}^0T)dx \approx wZ\exp(-E/\mathrm{R}^0T) = \frac{D_s}{u_c}Z\exp(-E/\mathrm{R}^0T).$$

From this equation we can then estimate the wave speed as

$$u_c = \sqrt{D_s Z \exp(-E/\mathrm{R}^0 T)} \tag{13}$$

and the combustion front thickness as

$$w = \sqrt{D_s \exp(E/\mathrm{R}^0 T)/Z} \tag{14}$$

The thickness of the wave front and the wave speed is a strong function of temperature. For the explosive material PBX 9501 at a temperature of 650K, the thickness of the combustion wave front is about 200 μm, and the combustion wave speed is 0.12cm/s. At temperature 2000K, the thickness becomes 56 Å and the wave speed becomes about 4 m/s. Besides, considering the gas composition inside the combustion front, the combustion wave speed is modified by a factor $\varphi$ as in Williams (1985):

$$\begin{aligned} u_c &= \phi\sqrt{D_s Z \exp(-E/\mathrm{R}^0 T_g)}, \\ \phi &= \frac{\sqrt{2}}{\beta}\left(1+\frac{1.344-3\alpha}{\beta}\right), \alpha = \frac{T_g - T_s}{T_s}, \beta = \frac{E(T_g - T_s)}{\mathrm{R}^0 T_s^2} \end{aligned} \tag{15}$$

where $T_s$ and $T_g$ are the solid and gas average local temperatures, $\beta$ is not smaller than 2. The examples on the thickness of the wave front suggest that it is impossible to resolve the temperature profile inside the combustion front. The speed of the combustion is apparently too low compared to the explosion wave. This wave speed is obtained by considering the heat conduction only. It is correct if the product gas can be removed quickly enough to prevent the heat convection induced by the gas motion. In typical cases, heat convection due to the motion of gas cannot be neglected. As mentioned before, solid explosives are typically porous material. The size of these pores is typically about 100 μm. It is also impractical for an engineering code to resolve gas and solid motions and heat transfers in such a small scale. To account for the various effects at such a small scale, we now introduced a subgrid model. We assume the pores are in a form of microtubes with radious $a$ (we use $a$ = 50 μm). The explosive material on the surface of the microtube has the temperature equal to the temperature of the gas phase. During an ignition process, the combustion wave burns in the radial direction into the solid explosive. The effective chemical reaction rate is determined by the volume swept by the combustion wave front traveling outward from the pore within a unit time. In this way we can then obtain the effective chemical reaction rate as a function of gas and solid volume fraction, to be used with Eq. (1):

$$R = Z \exp(-E/R^0 T_s) + 2\theta_g (u_c - u_s)/(\theta_s a) \tag{16}$$

Where $u_c$ is calculated by Eq. (15) with the gas temperature and $u_s$ is calculated by Eq. (15) with the solid temperature. The added $-u_s$ term is used to ensure that if the gas temperature is equal to the solid temperature, the usual Arrhenius law is recovered. With this chemical reaction rate model, combined the additional models discussed below, we can solve multiphase flow equations to predict the combustion wave speed. Depending on the temperature and construction of the explosion device, the typical chemical reaction wave speed is calculated to be a few hundred meters per second.

A model for the momentum coupling (drag between solid and gas) was obtained from the experimental results by Parker et al. (2003) for the temperatures below 453K. Above 453K, there is no available experimental data. However, near 453K, there is a noticeable thermal damage of the material. This damage may be the result of both chemical and physical processes like the decomposition of the binder in the solid explosive, volatilizing, or flowing as a result the squeezing effect from volume expansion of the material and solid-solid phase change of the crystals in the explosive (Parker, 2004). The drag coefficient for this

temperature range is estimated using the Ergun equation (Gidaspow, 1994). The coefficient in the Ergun equation is calibrated to match the experiment value at 453K. The momentum coupling coefficient $K_{gs}$ in Eqs. (4-5) is given by:

$$
\begin{aligned}
K_{gs} &= 8.6276\times 10^{8}, && T \le 293K \\
K_{gs} &= 8.6276\times 10^{8} - 5.38163\times 10^{6}(T-293), && 293K < T \le 453K \\
K_{gs} &= 288.26\frac{1-\theta_g}{\theta_g^2}\frac{\mu_g}{d_p^2} + 1.75\frac{\rho_g \,|\mathbf{u}_g - \mathbf{u}_s|}{\theta_g d_p} && T > 453K,\ \theta_g \le 0.8 \\
K_{gs} &= 0.75 c_d \frac{\rho_g \,|\mathbf{u}_g - \mathbf{u}_s|}{d_p}\theta_g^{-2.65}, && T > 453K,\ \theta_g > 0.8
\end{aligned}
\qquad (17)
$$

$$
\begin{aligned}
c_d &= \frac{24}{\mathrm{Re}_p}[1 + 0.15(\mathrm{Re}_p)^{0.687}], && \mathrm{Re}_p \le 1000, \\
c_d &= 0.44, && \mathrm{Re}_p < 1000, \\
\mathrm{Re}_p &= \frac{\theta_g \rho_g \,|\mathbf{u}_g - \mathbf{u}_s|\, d_p}{\mu_g}.
\end{aligned}
$$

Models for thermal coupling are less developed than the momentum coupling and there is no experiment data available. A model with a temperature range similar to the momentum coupling is proposed. The thermal coupling coefficient is calculated from the Nusselt number (*Nu*). For temperatures less than 293 K, the temperature difference is small, and the heat conduction is small. We use a large value ($10^4$) for the Nusselt number. We then let the Nusselt number drop to 10.0 quickly near temperature 453K. Above 453K, it is expected that the solid has experienced a lot of thermal damage and a formula based on thermal coupling for fluidized beds, (Kunii and Levenspiel, 1977), is used to give:

$$
\begin{aligned}
Nu &= 10^4, && T \le 293K \\
Nu &= 9999.596\,[1 - \exp(-0.038376(453 - T)] + 10, && 293K < T \le 453K, \\
Nu &= 10 - 0.4(T - 453), && 453K < T \le 473K, \\
Nu &= 0.03\,\mathrm{Re}_p,\ \mathrm{Re}_p = \frac{\rho_g \,|\mathbf{u}_g - \mathbf{u}_s|\, d_p}{\mu_g}, && T > 473K \\
K_e &= 6.0 K_g Nu/(d_p^2 \theta_g),
\end{aligned}
\qquad (18)
$$

*Nu* is not allowed to less than 2.0 to account for heat conduction.

Despite many uncertainties associated with the model, the qualitative results indicate a strong effect of the gas motion in the ignition process. The results are presented in Section 5.

## 4. Particle-in-cell method

As mention in the Introduction, to solve the equations listed above, a particle-in-cell method is needed. In this section we briefly introduce basics steps of the method. Detailed discussion about the method can be found in the paper by Cummins and Brackbill (2002) and the references cited.

Particle-in-cell method was originally developed by Francis Harlow (1971) in the early sixties. Despite its potential of accurately solving very difficult problems, it is numerically expensive compared to other methods for solving the Navier-Stokes equations. Its further development was delayed until the nineties when powerful computers became available. At

the same time computational fluid dynamics was matured enough to be applied to many engineering problems and more challenging problems such as fluid-structure interaction were being addressed. The particle-in-cell method has therefore become affordable and necessary in some of these cases.

In the particle-in-cell method, the material phase represented by particle is also represented on the grid. Each particle represents a piece of the material. Particle variables and the grid variables are related by shape functions $S_{pg}$ as in a finite element method. For instance, particle velocity $\mathbf{u}_p^{n+1}$ at time step n+1 is calculated as

$$\mathbf{u}_p^{n+1} = \mathbf{u}_p^n + \sum_{g=1}^{N} (\mathbf{u}_g^* - \mathbf{u}_g^n) S_{pg} \tag{19}$$

where N is the number of grid nodes comprising the cell in which the particle p resides and $\mathbf{u}_g^n$ is the velocity of the node at time step n. $\mathbf{u}_g^*$ is the newly calculated velocity on the grid node after the momentum equation is solved on the grid. If the particle method is not used, this velocity is the velocity on the grid at time step n+1. When the particle method is used, this velocity is modified according to the particle velocity and the new particle locations, so the grid velocity at time step n+1 is calculated as

$$\mathbf{u}_g^{n+1} = \frac{\sum_{p=1}^{N_p} m_p \mathbf{u}_p^{n+1} S_{pg}}{\sum_{p=1}^{N_p} m_p S_{pg}} \tag{20}$$

where $m_p$ is the particle mass, and $N_p$ is the number of particles in the cells surrounding node g. The particle position is updated every time step according to the particle velocity, and the shape functions are updated accordingly. It is important to note that in Eq (20) only the grid velocity difference is interpolated to the particle not the velocity itself. If the velocity, not the difference, is interpolated to the particle, it will cause undesired numerical diffusion. Other quantities, such as enthalpy, are calculated in the same way. The interpolations between particles and grid conserve the total physical quantities interpolated. The solid stress is a function of strain. The isotropic component of the stress on the particle is calculated as the summation of the pressure plus the product of the bulk viscosity and the strain rate, which can be calculated using the velocity at the current time step as

$$\dot{\boldsymbol{\varepsilon}}_p = \frac{1}{2} \sum_{g=1}^{N} (\mathbf{u}_g \cdot \nabla S_{pg} + \nabla S_{pg} \cdot \mathbf{u}_g) \tag{21}$$

This is similar to a finite element method. The gradient of the continuous field is calculated by taking gradients of the shape functions.

The deviatoric stress component $\boldsymbol{\tau}_p$ for the particle phase (for the case discussed in this paper, it is the solid stress $\boldsymbol{\tau}_s$) is calculated in the incremental form.

$$\boldsymbol{\tau}_p^{n+1} = \boldsymbol{\tau}_p^n + 2G\left(\dot{\boldsymbol{\varepsilon}}_p - \frac{1}{n_d} tr(\dot{\boldsymbol{\varepsilon}}_p)\mathbf{I}\right)\Delta t \tag{22}$$

where $G$ is the shear modulus, $\dot{\boldsymbol{\varepsilon}}$ is the strain rate tensor calculated using the velocity at the current time and $\Delta t$ is the time step, $n_d$ is the space dimension. A von Mises yield condition of the stress is enforced. We then calculate the effective stress as $\sqrt{\boldsymbol{\tau}_p^{n+1} : \boldsymbol{\tau}_p^{n+1}}$. If this stress is greater than the yield stress Y, then the deviatoric stress is normalized to the yield surface as

$$\boldsymbol{\tau}_p^{n+1} = \frac{Y}{\sqrt{\boldsymbol{\tau}_p^{n+1} : \boldsymbol{\tau}_p^{n+1}}} \boldsymbol{\tau}_p^{n+1}. \tag{23}$$

It is worth mentioning that this particle method is not restricted to the particular stress-strain model. Any constitutive relation that can be written in a differential form can be implemented into the particle method in a similar way on the particle because the particle is a Lagragian particle. For constitutive relations that are written in an integral form as encountered in some polymers, it may be necessary to store the strain rate for each particle for a sufficient number of time steps.

In the particle method the momentum equation is still solved on the Eulerian grid using the control volume method. The contribution of the solid stress to acceleration is calculated as

$$-\sum_{p=1}^{N_p} v_p \boldsymbol{\sigma}_p \cdot \nabla S_{pg} \Big/ \sum_{p=1}^{N_p} m_p S_{pg} \tag{24}$$

where $v_p$ is the particle volume and the minus sign comes from the fact that the gradient of the shape function is evaluated at the particle position. The numerator can be viewed as a total force contribution of the particles surrounding the grid point and the denominator is the total contribution of mass.

## 5. Numerical Results

To understand the basic behavior of solid explosive materials, we first numerically simulate the ignition of an explosive by a hot spot at the center of the material. We investigate the effect of the initial gas volume fraction. The solid explosives with initial gas volume fractions 2% and 5% are simulated. We perform a two-dimensional numerical simulation and use a one-inch (2.54cm) square of the explosive material (PBX 9501) with a uniform initial temperature of 300K, zero initial velocities and initial pressure of 50.33 MPa. Constant pressure $p_0$ of 50.33 MPa (497 atmosphere pressure) is applied on the four sides of the solid explosive to simulate an ignition under a higher pressure.. A computational cell at the center is heated by a heat source from t = 0 to t = 0.0001 S to reach an *initial hot spot temperature.* Then the heat source is removed and the simulation is run to t = 0.01 S. There are two distinguished cases. In one of the cases, there is not any significant reaction, and at the end, there is only some trace of gas volume fraction. This case is termed as "NO GO" case. In another case, there is a strong chemical reaction during the run, and shortly after it, all the solid mass is consumed, this is a "GO" case. A computational domain of 22 nodes by 22 nodes is used. The critical temperature Tc is defined as the initial hot spot temperature that separates the "GO" and "NO GO" cases. The critical temperature Tc for an explosion is found to be 599K for the case of 2% initial gas volume fraction and to be 584K for the case of 5% gas volume fraction. These results imply that at a higher porosity the explosive material is more sensitive to a hot spot. This is consistent with experimental observations that damaged explosives are more sensitive for non-shock initiations. The gas motion in pores of the solid explosive significantly enhances heat transfer. This effect can be understood as significant effective conductivity increase in the porous material. Although Eq. (15) cannot be used directly to calculate the combustion wave speed in the case, it indicates significant combustion wave speed increase in the porous material. As solid converted to gas in the combustion process, the porosity is further increased and results in increasingly larger combustion wave speed as the ignition progresses. This is indeed observed in the following example in Fig. 2, which shows an example with initial gas volume fraction of 2% and an initial temperature of 601K (a "GO" case). The development of the chemical reaction is slow at the initial stage. Significant gas production is not observed until 7.510 ms later. About 2 μs later significant gas production is observed. In about another microsecond all the explosive material is consumed. The combustion wave speed changes from less than a centimeter per second to a few kilometers per second in a short period of a few microseconds. From Fig 2, on can estimate the combustion wave speed to be about 5 km/s. The longitudinal elastic wave speed in this explosive material is less than 3 km/s. The combustion wave speed is supersonic. This example shows the significant time scale change in the explosive process.

This change of scales poses a significant challenge in the theoretical modeling and numerical simulation. Given the apparently difficulties in experiment with this material, we caution ourselves that many parameters used in our numerical simulation are the best guesses at this time.

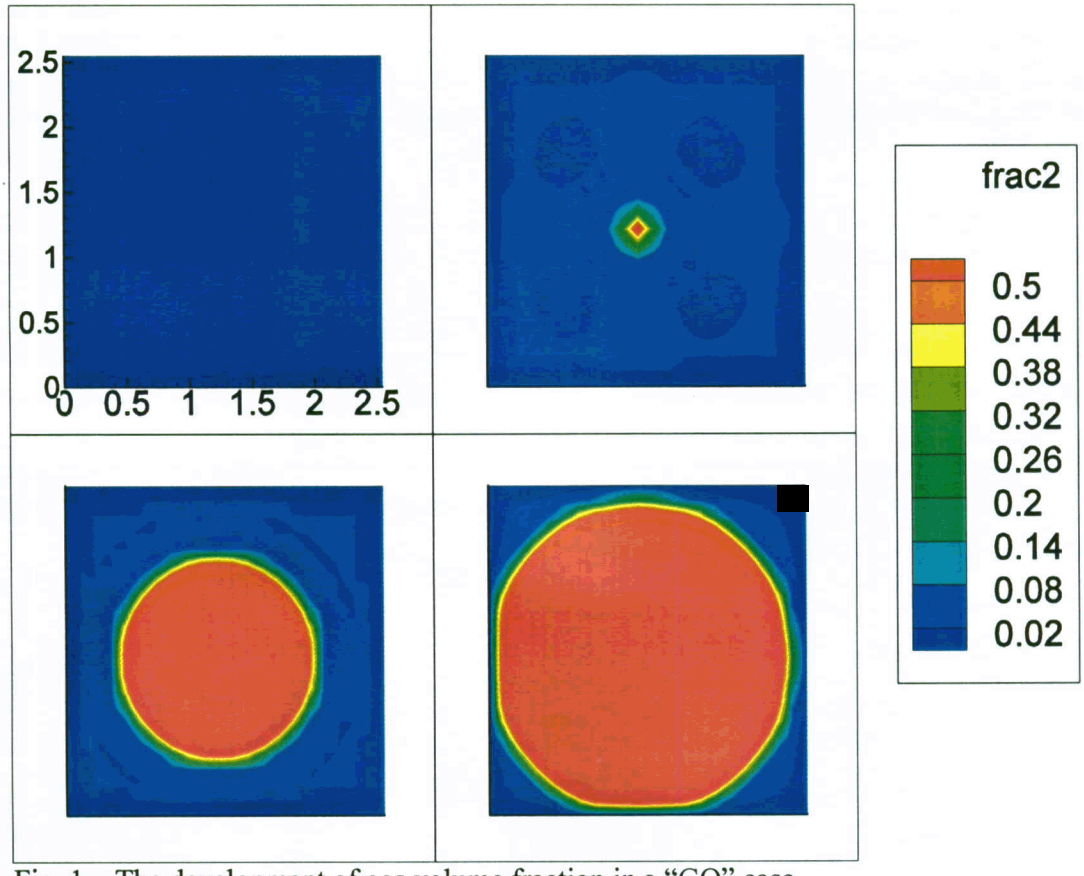


Fig. 1 The development of gas volume fraction in a "GO" case.
Top left: t = 0.0 s, top right: t = 7.5100 ms,
Bottom left: t = 7.5120 ms, bottom right: t = 7.5127 ms.

Although Fig. 1 shows reasonable explosion process, the two-phase flow model introduced in this paper is only intended to simulate the ignition of an explosion in the material, not to simulate the progress of the explosion. As we mention above, after the explosive material is ignited the progress of the explosion is rapid, the temperature can reach a few thousand degree. At this stage the thermal radiation becomes an important heat transfer mechanism. This effect is not accounted for in the model introduced in this paper.

The second example is part of our effort in the simulation of the experiment of Dyer and Taylor (1970). The setup of the experiment is shown in Fig. 2. A one inch cube of a high explosive material (HE) is pressed onto a plate. The plate is suddenly given a velocity of 6 m/s for 0.01 second. Depending on the material on the surface of the moving plate and pressure imposed on the explosive, explosions are sometime observed.

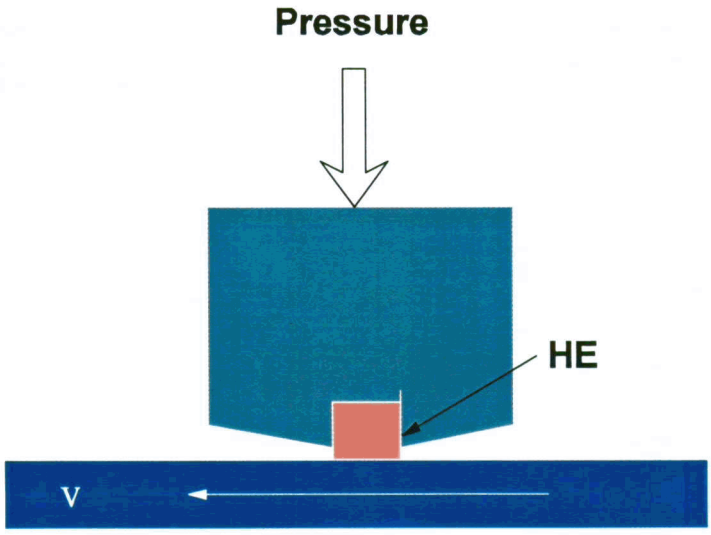


Fig. 2, The Dyer and Taylor experiment.

The experiment indicates that the heat generation around the sand grits on the surface is an important mechanism for the ignition of the explosive material. Interactions of the sand grit, mostly through interactions motion of gas around the grits, significantly enhance the tendency of explosion. To numerical study the interactions of the hot spots generated around sand grits, we perform a two-dimensional numerical simulation according the conditions described in the paper. A one-inch (2.54cm) square of the explosive material is with a uniform initial temperature of 300K is bounded by three (left, right and top) adiabatic walls. The normal velocities on these walls are set to be zero. The bottom boundary is also adiabatic. The normal velocities of the solid and the gas phases are set to zero. To mimic the effect of the gas produced by chemical reactions at the early stage of the experiment, and the effect of sliding plate, the tangential gas velocity on the bottom is set to be the plate velocity, and the momentum coupling and energy coupling between the solid phase and the gas phase is reduced in the first layer of the computational cells near the plate. The initial pressure on the system is 50.33 MPa according to the applied pressure in the experiment.

Fig. 3 shows the comparison of results with one initial hot spot (left) and two initial hot spots (right). The initial hot spots are generated by heat flux from t = 0 to t = 0.0001 S to reach a initial hot spot temperature of 641K. In both cases, the gas velocity on the bottom is set to 6 m/s parallel to the plate. In the case with two pot spots, the distance between the hot spots is about 0.5 cm. The figure shows the temperature contour at 5 ms into ignition process. At this time, the maximum gas temperature of the single hot spot case is 620K, that does not lead to an explosion, while the maximum gas temperature of the two-hot-spot case is 1125K, which eventually leads to an explosion. From more runs, we found that the critical temperature Tc is 643K for the single hot spot case and is 639K for the two-hot-spot case. With the gas motion at the bottom layer, the two-hot spot case is more sensitive. The gas motion in the single hot spot case carries away heat generated from the chemical reaction and reduces the tendency of explosion. With two hot spots, the down stream hot spot is heated by the hot gas generated from the upstream one and develops into an explosion.

To study the effects of sliding velocity, we have also simulated the cases without the sliding velocity but with reduced momentum coupling and energy coupling at the bottom as for the sliding cases. The critical temperature for the single hot spot case reduces to 623K, while the critical temperature for the two hot spot case remains at 639K. Without gas motion at the bottom layer the tendency of explosion is reversed from the cases study above with gas motion at the bottom. This is because in the two-hot spot case, the combined pressure generated at both hot spots help each other lift the explosive material up near the hot spots and the solid material near the heat region moves away from it and reduced the tendency of explosion. In the two-hot-spot case with sliding, there are two competing factors: on one hand, sliding carries away hot gas from the not spots, on the other hand, the downstream hot

spot receives some hot gas swept from the upstream hot spot. Thus, it looks that these two factors act together to keep Tc unchanged from the case without plate sliding.

Fig. 4 shows the particle state at time 0.00512 S for the case of two initial hot cells, the region with blue color is a burned region, with small solid mass. The velocity of the solid phase follows the gas velocities there due to momentum coupling.

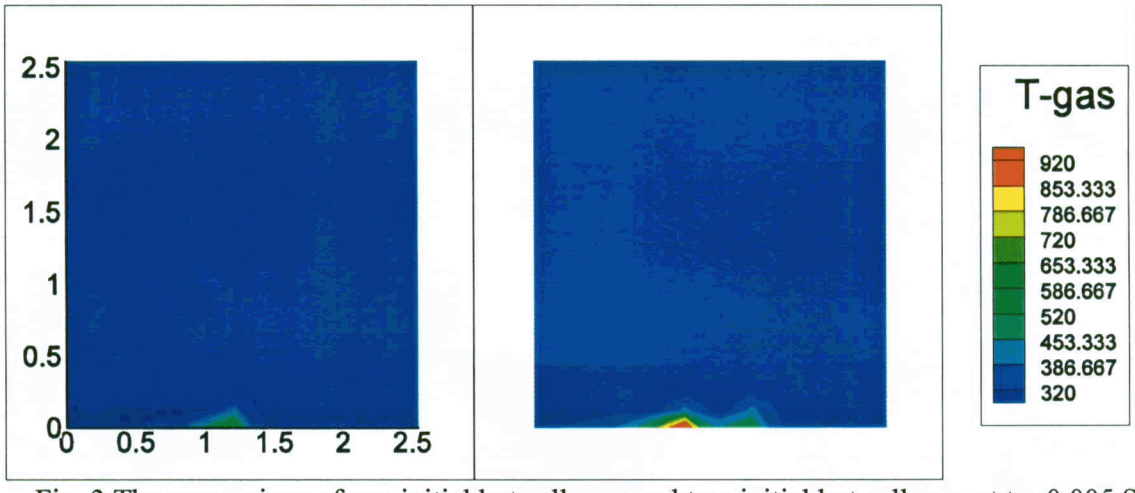


Fig. 3 The comparison of one initial hot cell case and two initial hot cell case at t = 0.005 S, left: one hot cell, right: two hot cells. The gas temperature is shown.

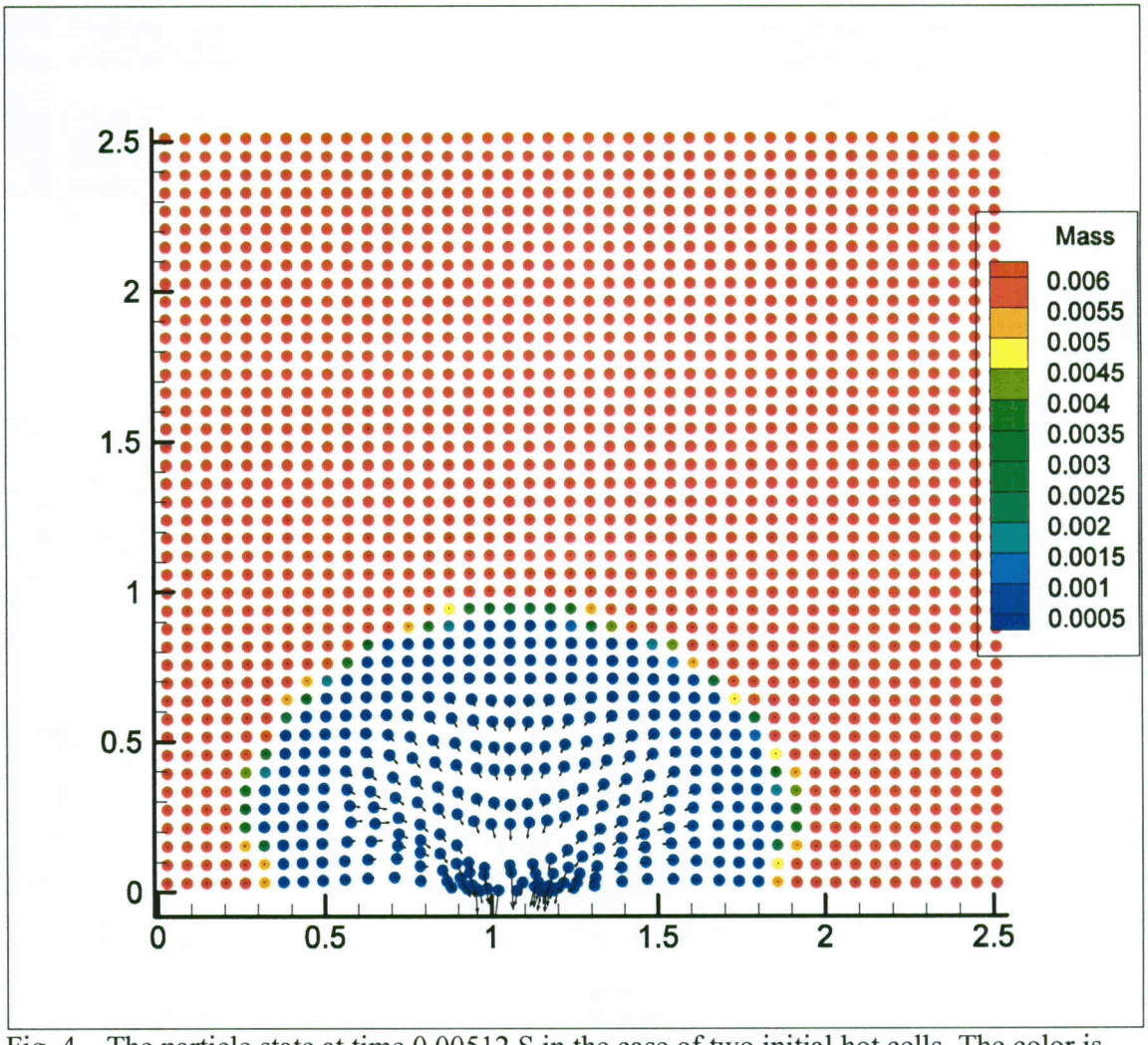


Fig. 4 The particle state at time 0.00512 S in the case of two initial hot cells. The color is from particle mass. The arrows indicate velocities.

## 6. Summary

A computational paradigm with particle-in-cell method coupled with flow in discussed, A subgrid model of the chemical reaction is presented, a careful momentum, energy coupling is studied. Some computational results related to high explosive are presented.

Our immediate future plans include testing the link between our ignition temperature model and our reactive multiphase flow simulation on the experiments of Dyer and Taylor (1970) and Randolph, et al (1976). We also plan to work with the experimental group, DX-2 at the Los Alamos National Lab to try to better understand and improve the assumptions made in our ignition temperature model. This will include detailed simulations of the local behavior near a grit particle.

## References

Barenblatt, G. I., 1996, Scaling, self-similarity, and intermediate asymptotics, Cambridge University Press.

Bennett, J. G. Haberman, K. S., J. N. Johnson, B. W. Asay and B. F. Henson, 1998, A

Constitutive Model for the Non-shock Ignition and Mechanical Response of High Explosives. J. Mech. Phys. Solides, Vol. 46, No. 12, pp. 2303-2322.

Browning, R. V., Peterson, P. D., Roemer, E. L. Scammon, R. J., 2003, Grit particle enhanced non-shock ingnition of explosives Los Alamos National Lab Report, LA-UR-03-1840.

Boddington, T., The growth and decay of hot spots and the relation between structure and stability, 1962, Ninth Symposium on Combustion, pp. 287-293.

Cummins, S.J, and Brackbill, J.U. 2002, An implicit particle-in-cell method for granular materials, J. Appl. Comput. Phys. **180**, 506-548.

Dick, J.J, Martines, A.R. and Hixson. R. S., 1998, Plane impact response of PBX 9501 and its components below 2 GPa. Los Alamos National Lab Report, LA-13426-MS.

Dyer, A. S., and Taylor, J. W., Initiation of detonation by friction on a high explosive charge, 1970, Proceedings of 5th Symposium on detonation.

Gibbs, T. R. and Popolato, A., 1980, LASL Explosive Property Data, University of California Press.

Gidaspow, D., 1994, *Multiphase Flow and Fluidization*, Academy Press, p151.

Guilkey, J., Harman, T. B., Kashiwa, B. A. and McMurtry, P. A., 2004, An Eulerian-Lagrangian Approach for Large Deformation Fluid Structure Interaction Problems. Preprin.

Hackett, R. M. and Bennett, J. G., 2000, An Imicit Finite Element Mterial Mdel for Eergetic Particulate Composite Materials. Int. J. Numer. Mech. Engng 49:1191-1209.

Harlow, F.H. and Amsden, A.A. 1971, Fluid Dynamics — A LASL Monograph, Los Alamos National Lab Report, LA-4700.

Henson, B. F. Smilowitz, L., Asay, B. W. and Dickson, P. M., 2002, A model of thermal decomposition and ignition in HMX, , Los Alamos National Lab Report, LA-UR-02-1945.

Incropera, F. P., 1990, Fundamental of Heat and Mass Transfer, 3rd edition, John Wiley & Sons.

Kang, J. and Butler, P. B., 1992, A Thermomechanical Analysis of Hot Spot Formation in Condensed-Phase, Energetic Materials, Combust. Flame, 89, pp 117-139.

Kunii, D., and Levenspiel O., 1977, *Fluidization Engineering,* Robert E. Krieger, p 217.

Lyman, J. L., and Liau, Y.C., 2002, Thermochemical Functions for Gas-Phase, 1,3,5,7-Tetranitro-1,3,5,7-tetraazacyclooctane (HMX), Its Condensed Phases, and Its Larter Reaction Products, Combust. Flame, 130, pp 185-203..

Mellor, A. M., Wiegand, D. A. and Isom, K. B., 1995, Hot Spot Histories in Energetic Materials, Combust. Flame 101: 26-35.

Menikoff, R and Sewell, T. D., 2002, Constituent properties of HMX needed for mesoscale simulations, Combust. Theory Modeling 6, 103-125.

Parker, G. R., Asay, B. W, Dickson, P. M., Henson, B. F., Smilowitz, L. B., 2003, of Thermal Damage on the Permeability of PBX 9501, *Shock Compression of Condensed Matter, American Physical Society Topical Conference*, Portland, OR, July 20-25.

Parker, G. R., 2004, Private communication.

Randolph, A. D., Hatler, L.E., and Popolata, A., Rapid heating-to-ignition of high explosive. I. Friction heating, 1976, *Ind. Eng. Chem. Fundam.* **15**(1), 1-6.

Williams, F. A., 1985, *tion Theory: The Fundamental Theory of Chemically Reacting Flow Systems*, 2nd Edition, Addison-Wesley, p159.

VanderHeyden, W. B., Dendy, E. D., Padial-Collins, N. T., 2000, Catablanca-A Pure-Java, Component-based systems Simulation Tools for Coupled Nonlinear Physics on Unstructured Grids-An Update, Los Alamos National Lab Report, LA-UR-00-6049.

## Appendix. Constants used

Listed are values of the physical quantities used in the simulation. The temperature dependence of the value is not considered at the time. The value for the gas is based on an assumption that it is formed by $4N_2 + 4H_2O + 4CO$. The values are from Dick et al. (1998), Gibbs and Popolato, (1980), Incropera (1990), Henson et al. (2002), Lyman and Liau (2002).

$Z$: Arrhenius pre-exponential. 5.5788E12 1 / s.

E: Activation energy, 149000 J / mole.

R: gas constant, 8.31439 J / mole-K

$C_{ps}$: Specific heat for PBX 9501, $1.717\times10^3$ J / kg-K,

$C_{pg}$: Specific heat for the gas, $1.507\times10^3$ J/ kg-K.

$T^f$: Temperature formation. 298.0 K for both solid phase and gas phase.

$h_s^f$: Enthalpy formation for the HE, 1400.

$h_g^f$: Enthalpy formation for the gas, 0.

$\mu_g$: Gas viscosity, $2.406*10^{-5}$ Ns/m$^2$.

$K_g$: Gas thermal conductivity, $5.652*10^{-2}$ J/S-m-K.

$d_p$: Particle diameter, $10^{-4}$ m.

$E_s$: Young's Modulus of the solid, $9.575\times10^3$ MPa.

$\nu$: Poisson ratio of the solid, 0.36.

$B$: Bulk modulus of the solid, $B = \dfrac{E_s}{3(1-2\nu)}$.

G: Shear modulus of the solid, $G = \dfrac{E_s}{2(1+\nu)}$.

$\mu_2$: Bulk viscosity of the solid, $5.0\times10^{-4}$ MPa-S.

$\mu$: Shear viscosity of the solid, $5.0\times10^{-4}$ MPa-S.

*eosA*: A constant in the equation of state of the solid, 1829.984 kg/m$^3$.

*eosB*: A constant in the equation of state of the solid, 0.160526 kg/(m$^3$MPa).

$B_g$: A constant in the equation of state of the gas, 2937.8 kg/(m$^3$MPa).